A Computational Study of Intramolecular Proton Transfer in Gaseous Protonated Glycine

Kui Zhang and Alice Chung-Phillips*

Department of Chemistry, Miami University, Oxford, Ohio 45056

Received September 18, 1998

The minimum energy paths for intramolecular proton transfer between the amino nitrogen and carbonyl oxygen atoms in gaseous protonated glycine were estimated at the Hartree−Fock (HF) and second-order Møller−Plesset Perturbation (MP2) levels of theory. Potential energy profiles and their associated reactant, transition state, and product species calculated at the MP2/6-31G* level were shown to differ significantly from those obtained at the HF/6-31G* level. Effects of electron correlation and basis functions on the calculated geometries and energies of relevant species were examined at the HF, MP2, MP4, CCSD, and B3LYP levels using the 6-31G*, 6-31G**, 6-31+G**, 6-311+G**, 6-31+G(2d,2p), 6-311+G(3df,2p), cc-pVDZ, aug-cc-pVDZ, and cc-pVTZ basis sets. The HF and MP2 optimized levels with the 6-31G*, 6-31G**, 6-31+G**, and 6-311+G** bases were used to calculate the thermodynamic and kinetic properties of the proton transfer reaction at 298.15 K and 1 atm, which include enthalpy, entropy, Gibbs free energy, equilibrium constant, potential energy barriers, tunneling transmission coefficients, and rate constants. Results indicate that the proton in a carbonyl O-protonated glycine undergoes a rapid migration to the amino nitrogen atom, while the reverse process is extremely unfavorable. The objective of this work is to develop practical theoretical procedures for studying proton transfer reactions in amino acids and peptides and to assemble physical data from these model calculations for future references.

INTRODUCTION

Both protonation and proton transfer play important roles in biological processes.[1−5] In a biomolecule there are many possible protonation sites, and a proton can transfer from one site to another. For this reason proton transfer is a fundamental phenomenon in a wide range of biological reactions, and it is important to gain a basic understanding of this process.

One of the means to investigate proton transfer is the application of ab initio molecular orbital (MO) method. But to apply such a rigorous treatment on a large system like protein is not possible with the present computer power, nor will it be possible in the near future. A practical solution is to study model compounds which have the essential structural characteristics of the real system and are suitable for ab initio calculations. In recent years several ab initio studies have been carried out on proton transfer in a variety of model systems.[6−14]

Glycine, H_2NCH_2COOH, is a meaningful model for amino acids and peptides. Glycine (Gly) and its protonated species ($GlyH^+$) have been thoroughly investigated by experimental and theoretical methods.[15−31] As regards the mechanism for intramolecular proton transfer, an ab initio study on the formation of glycine zwitterion in aqueous solution, $H_3N^+CH_2COO^-$, was reported recently.[26] But for protonated glycine, there appeared only one semiempirical MO treatment.[15] It is therefore an opportune time to conduct a more rigorous study on this subject.

Recently we completed two high-level ab initio investigations on glycine and related model systems: a benchmark calculation of the gas-phase basicity (GB) of Gly and an analysis of the conformational potential energy surface (PES) of gaseous $GlyH^+$.[29,31] In this work we apply the Hartree−Fock (HF) and second-order Møller−Plesset Perturbation (MP2) levels of theory to determine the electronic structures and physical properties associated with the intramolecular proton transfer in gaseous $GlyH^+$. The objective is to develop practical ab initio procedures and provide reliable physical data for future research on amino acids and peptides.[24,29,31−33]

COMPUTATIONAL METHODS

There are three possible protonation sites in Gly: the amino nitrogen atom and the carbonyl and hydroxyl oxygen atoms of the carboxyl group. Based on previous ab initio calculations, the amino nitrogen is energetically preferable to the carbonyl oxygen as a protonation site, whereas protonation on the hydroxyl oxygen leads to a stable ion−dipole complex with high energy.[19,21,27] Therefore, it is energetically favorable for the proton in $GlyH^+$ to migrate from the oxygen to the nitrogen atom, with the carbonyl O-protonated species $H_2NCH_2C(OH)_2^+$ as the reactant $GlyH^+$(O) and the amino N-protonated species $H_3N^+CH_2COOH$ as the product $GlyH^+$(N). Accordingly, the forward reaction is

$$GlyH^+(O) \rightarrow GlyH^+(N) \quad (1)$$

while the reverse reaction is

$$GlyH^+(N) \rightarrow GlyH^+(O) \quad (2)$$

The path of proton transfer is expected to follow the bridging

* To whom correspondence should be addressed.

10.1021/ci9802225 CCC: $18.00 © 1999 American Chemical Society
Published on Web 02/18/1999

arrangements N···H−O (reactant) ↔ N···H···O (TS) ↔ N−H···O (product) via the transition state $GlyH^+$(TS). But the TS from the MP2 optimization procedure will be shown to be different from what is expected: it has the structure of an O-protonated species N···H−O (TS) instead of a molecular complex N···H···O (TS) (*vide infra*).

The search for the proton-transfer path began with the selection of likely pairs of reactant/product structures obtained previously at the HF/6-31G* and MP2/6-31G* levels.[19,31] A pair was subjected to further tests when a TS was located by applying (a) the linear synchronous transit (LST) method[34] followed by a TS geometry optimization or (b) by a direct TS geometry optimization using an initial geometry with the proton placed between the oxygen and nitrogen atoms. Each optimized TS structure was shown to possess only one imaginary vibrational frequency. To confirm that the proposed structures were all connected by the path, calculations of intrinsic reaction coordinate (IRC)[35] were carried out from the TS stepping downhill in two opposing directions on the PES, using mass-weighted internal coordinates with a step size of 0.1 $amu^{1/2}$ bohr for HF/6-31G* and 0.3 $amu^{1/2}$ bohr for MP2/6-31G*. (An increase in basis size or a decrease in step size would require unreasonably large computing resources.) If the resulting IRC linked the TS to a reactant/product pair of physically reasonable geometries (via possible intermediates), the path was established.

Calculations were carried out with the Gaussian program.[36,37] Electronic structures for the species in the proton transfer path were obtained by geometry optimizations at the HF and MP2 levels of theory using the 6-31G*, 6-31G**, 6-31+G**, and 6-311+G** basis sets. These are standard double and triple split-valence sets including polarization and diffuse functions. Harmonic vibrational frequencies were calculated at these levels for deriving the thermodynamic and kinetic properties of the proton transfer reaction. Single-point (SP) calculations were also performed using the MP2, MP4, CCSD (coupled-cluster including all single and double excitations[38]), and DF (density functional[39]) theories, standard sets extended with higher polarized functions, and the Dunning[40] correlation-consistent polarized split-valence bases (cc-pVXZ) augmented with diffuse functions (aug-cc-pVXZ). Except for evaluating the CCSD T1 diagnostic,[41] tight HF convergence and full correlation treatment were applied, i.e., SCF = Tight, MP2 = Full, MP4 = Full, and CCSD = Full. Optimization to a TS required analytic HF force constants and suppression of Berny curvature testing, i.e., Opt = (TS,-Calcall,Noeigentest).

PHYSICAL PROPERTIES

For the proton transfer reaction 1, several physical properties defined below are deduced. The major change is the electronic energy at 0 K:

$$\Delta E_e = E_e[GlyH^+(N)] - E_e[GlyH^+(O)] \quad (3)$$

Standard thermodynamic quantities for the gas-phase reaction at temperature *T*, including changes in enthalpy, entropy, and Gibbs free energy, are calculated from the equations

$$\Delta H^\circ = \Delta E_e + \Delta E_{ZP} + \Delta(E - E_0) \quad (4)$$

$$\Delta S^\circ = S^\circ[GlyH^+(N)] - S^\circ[GlyH^+(O)] \quad (5)$$

$$\Delta G^\circ = \Delta H^\circ - T\Delta S^\circ \quad (6)$$

where ΔE_{ZP} and $\Delta(E - E_0)$ are differences in zero point energies and thermodynamic internal energy, respectively. (Note: $E_0 = E_e + E_{ZP}$.) For the chemical system at equilibrium

$$GlyH^+(O) \rightleftharpoons GlyH^+(N) \quad (7)$$

the equilibrium constant is

$$K_p = \exp[-\Delta G^\circ/(RT)] \quad (8)$$

The classical rate constants for the forward and reverse reactions 1 and 2 are calculated by means of the conventional transition state theory (TST).[17,42] The equation for the rate constant k^{TST} is

$$k^{TST} = \frac{k_B T}{h}\frac{Q^\ddagger}{Q^R} e^{-\Delta E_0^\ddagger/(k_B T)} \quad (9)$$

Here k_B and h are the Boltzmann and Planck constants; $Q^\ddagger$ and Q^R are the equilibrium partition functions for the TS and reactant, and $E_0^\ddagger$ is the barrier height corrected for zero point energy

$$\Delta E_0^\ddagger = (E_e^\ddagger + E_{ZP}^\ddagger) - (E_e^R + E_{ZP}^R) \quad (10)$$

(Note: $\Delta E_0^\ddagger = E_0^\ddagger - E_0^R$) In addition, the quantum mechanical tunneling effect is approximately taken into account via a tunneling transmission coefficient κ with the expression[17,43]

$$\kappa = 1 - \frac{1}{24}\left(\frac{h\nu^\ddagger}{k_B T}\right)^2\left(1 + \frac{k_B T}{\Delta E_0^\ddagger}\right) \quad (11)$$

where $\nu^\ddagger$ is the imaginary frequency at the transition state. Including the tunneling effect, the final rate constant k is given by

$$k = \kappa k^{TST} \quad (12)$$

The minimum energy path (MEP) for the proton transfer reaction is approximated by the IRC obtained at the HF/6-31G* and MP2/6-31G* levels. (The IRC has been used previously to represent the MEP.[44]) For a given reaction, the MEP is defined as the combination of the steepest descent paths in the mass-weighted cartesian coordinates from the TS to the reactant and to the product. The distance along the MEP is represented by the reaction coordinate *s*, which is zero at the TS, positive in the product direction, and negative in the reactant direction.

The existence of a MEP shown explicitly for the HF/6-31G* or MP2/6-31G* structures is the basis for assuming the existence of a comparable MEP that connects the corresponding structures refined by geometry optimizations with a larger basis set (6-31G**, 6-31+G**, or 6-311+G**) at the respective HF or MP2 level. This assumption is likely to be valid considering the similarities in the $GlyH^+$ geometries and vibrational frequencies obtained from the four basis sets (cf. Tables 2 and 3 and S2 and S3 below). The

Table 1. Relative Electronic Energies for Protonated Glycine Structures Calculated at Different Levels[a]

At the HF Optimized Geometries

level[b]	L2 (energy)	L1 (geometry)	$GlyH^+$(O)	$GlyH^+$(TS)	$GlyH^+$(N*)	$GlyH^+$(N)
f1	HF/6-31G*	HF/6-31G*	13.81	19.45	0.54	0.00
f2	HF/6-31G**	HF/6-31G**	11.11	16.29	0.37	0.00
f3	HF/6-31+G**	HF/6-31+G**	11.49	16.98	0.44	0.00
f4	HF/6-311+G**	HF/6-311+G**	11.90	17.33	0.51	0.00
f5	MP2/6-31+G**	HF/6-31+G**	15.16	12.29	−0.09	0.00
f6	MP4/6-31+G**		14.78	12.87	−0.14	0.00
f7	MP2/6-31+G(2d,2p)		14.85	11.48	−0.39	0.00
f8	"MP4/6-31+G(2d,2p)"		14.47	12.06	−0.44	0.00
f9	MP2/aug-cc-pVDZ	HF/6-31+G**	13.89	10.82	−0.28	0.00
f10	B3LYP/6-311+G**	HF/6-311+G**	12.04	10.47	−0.61	0.00
	MP2/6-31G*	HF/6-31G*	17.60	14.16	−0.25	0.00
	MP3/6-31G*		15.61	15.14	−0.13	0.00
	CCSD/6-31G*		16.10	15.53	−0.11	0.00
	MP4/6-31G*		17.26	14.98	−0.27	0.00
	(CCSD T1 diag)[c]		(0.014)	(0.014)	(0.014)	(0.013)

At the MP2 Optimized Geometries

level	L2 (energy)	L1 (geometry)	$GlyH^+$(O)	$GlyH^+$(TS)	$GlyH^+$(N)
m1	MP2/6-31G*	MP2/6-31G*	35.74	40.59	0.00
m2	MP2/6-31G**	MP2/6-31G**	32.59	37.47	0.00
m3	MP2/6-31+G**	MP2/6-31+G**	32.03	36.61	0.00
m4	MP2/6-311+G**	MP2/6-311+G**	30.39	34.80	0.00
m5	MP4/6-311+G**		29.95	34.37	0.00
m6	MP2/6-311+G(3df,2p)		29.20	33.66	0.00
m7	"MP4/6-311+G(3df,2p)"		28.76	33.23	0.00
m8	MP2/cc-pVDZ	MP2/cc-pVDZ	30.86	35.80	0.00
m9	MP2/cc-pVTZ	MP2/6-311+G**	29.03	33.67	0.00
m10	B3LYP/6-311+G**	MP2/6-311+G**	26.91	32.08	0.00

[a] Unit: ΔE_e in kcal/mol. Data for E_e are provided in Table S1. [b] Level is L2//L1. A blank L1 implies the same L1 as above. For the composite level "L2", $E_e(f8) = E_e(f6) + E_e(f7) - E_e(f5)$ at the f5 geometries, and $E_e(m7) = E_e(m5) + E_e(m6) - E_e(m4)$ at the m4 geometries. [c] Based on CCSD(fc)/6-31G* T1 diagnostic (ref 41).

assumption is further supported by separate calculations on the protonated formamide [Appendix A1]. Thus the thermodynamic and kinetic properties for the proton transfer reaction may be deduced from the physical properties of the relevant species calculated from any of the four basis sets, while those from the largest set 6-311+G** should be taken as the best values.

STRUCTURAL REPRESENTATIONS

Several $GlyH^+$ conformers were previously obtained by geometry optimizations at the HF/6-31G* level by Jensen[19] and at the MP2/6-31G* correlated level by the present authors.[31] In this work we began with the known conformers to determine the lowest-energy proton-transfer path by the LST and IRC methods as described above. The resulting product/reactant pairs are structures **1**/**2** for HF and **3**/**4** for MP2 in Figure 1 (top row). (These correspond to structures H1/H4 and 1m/6m in refs 19 and 31, respectively.) In the figure the origin and destination of each proton transfer are shown by a connecting dashed line. Two analogous pairs of protonated diglycine ($GlyGlyH^+$) found previously at the HF/6-31G* level are **5**/**6** and **7**/**8** in Figure 1 (bottom row).[24]

There is a problem in the conformations of the structures determined with and without electron correlation, i.e., the HF pair **1**/**2** appears entirely different from the MP2 pair **3**/**4**. The conformations of the global minima **1** and **3** are related by a simple internal rotation around the C−N bond. After correcting for zero-point vibrations, the energies between two such conformations are nearly the same (within 0.5 kcal/mol) on either the HF PES or the MP2 PES.[19,31] Thus the difference between 1 and 3 is not serious with respect to both geometry and energy. The problem lies in the O-protonated species: **2** is nonexistent at the MP2 PES while **4** is nonexistent at the HF PES. The MP2/6-31G*//HF/6-31G* energy of **2** is *ca.* 18 kcal/mol below the MP2/6-31G*//MP2/6-31G* energy of **4**, which implies that HF has predicted a much more stable O-protonated species than MP2. On the basis that MP2 geometries are generally more reliable than HF geometries and no MP2 conformer anywhere close to **2** has been found,[31] we deduce that **2** is unstable in the gas phase. In an aqueous solution where intermolecular interactions play a significant role in stabilizing different forms of $GlyH^+$, there is a possibility that **2** exists. A recent MP2/6-31+G** calculation[26] on Gly (aq) showed a similar intramolecular proton transfer path N···H−O → N···H···O → N−H···O, where the reactant has the conformation of the second most stable Gly (g) (e.g., IIn of ref 20) while the product is the zwitterion.

In light of the instability of the $GlyH^+$ structure **2**, we now focus on the stability of the $GlyGlyH^+$ structures **6** and **8**. The N-terminus $GlyH^+$ residue in **6** is expected to be more stable than **2** because the carbonyl O atom is more basic in an amide group than in a carboxylic group.[7] This is consistent with a larger experimental GB for formamide (189.1 kcal/mol for O-protonation) than formic acid (169.8 kcal/mol). (The experimental values refer to the current NIST standard reference values.[45]) Likewise, the C-terminus $GlyH^+$ residue in **8** is expected to be more stable than **2** because the proton bonded to the O atom is less likely to be extracted by an amide N than an amino N atom. Again, this is consistent

Table 2. Geometrical Parameters for Protonated Glycine Structures Optimized at the HF/6-311+G** and MP2/6-311+G** Levels[a]

	HF/6-311+G**				MP2/6-311+G**		
	$GlyH^+$(O)	$GlyH^+$(TS)	$GlyH^+$(N*)	$GlyH^+$(N)	$GlyH^+$(O)	$GlyH^+$(TS)	$GlyH^+$(N)
C2−C1	1.507	1.517	1.520	1.517	1.506	1.490	1.525
O3−C1	1.249	1.220	1.181	1.179	1.287	1.286	1.210
O4−C1	1.258	1.266	1.296	1.299	1.277	1.274	1.319
H5−O4	0.955	0.953	0.951	0.951	0.977	0.978	0.972
N6−C2	1.441	1.466	1.501	1.495	1.442	1.467	1.498
H7−C2	1.085	1.082	1.080	1.081	1.092	1.091	1.090
H8−C2	1.085	1.082	1.080	1.081	1.093	1.097	1.091
H9−N6	0.999	1.003	1.009	1.009	1.012	1.013	1.023
H10−N6	0.999	1.003	1.009	1.011	1.012	1.013	1.024
H11−N6 (H11···N6)	(1.987)	(1.354)	1.019	1.011	(3.334)	(2.882)	1.033
H11−O3 (H11···O3)	0.970	(1.160)	(2.013)	(2.510)	0.972	0.974	(2.075)
O3−C1−C2	120.3	114.4	121.2	121.0	124.8	122.8	121.0
O4−C1−O3	119.3	119.7	111.3	111.3	117.7	119.6	110.9
H5−O4−C1	114.7	113.7	111.8	111.7	112.5	112.5	109.2
N6−C2−C1	107.8	101.7	107.2	107.3	110.3	108.7	105.9
H7−C2−C1	106.9	109.9	110.6	111.2	107.9	107.8	112.5
H8−C2−C1	106.9	109.9	110.6	111.2	109.3	108.0	109.9
H9−N6−C2	113.2	113.6	112.4	111.8	114.7	111.2	112.9
H10−N6−C2	113.2	113.6	112.4	110.9	115.7	115.8	111.7
H11−N6−C2		(90.1)	107.9	110.9			107.4
H11−O3−C1	108.6	(96.8)			112.5	112.5	
O4−C1−C2−O3	180.0	180.0	180.0	180.0	−174.1	−176.9	178.9
H5−O4−C1−O3	0.0	0.0	0.0	0.0	−0.9	0.1	1.4
N6−C2−C1−O3 (ψ_2)	0.0	0.0	0.0	0.0	95.4	70.0	10.9
H7−C2−C1−N6	122.9	120.2	119.6	119.0	120.4	122.4	120.3
H8−C2−C1−N6	−122.9	−120.2	−119.6	−119.0	−121.5	−120.5	−117.4
H9−N6−C2−C1	−118.0	−117.6	−119.2	179.9	67.0	123.1	−151.3
H10−N6−C2−C1 (ψ_1)	118.0	117.6	119.2	58.6	−65.6	−1.0	86.6
H11−N6−C2−C1		(0.0)	0.0	−58.6			−29.7
H11−O3−C1−C2	0.0	(0.0)			8.3	4.6	

[a] See Figures 2 and 3 for atom numbers and Table S2 for parameters of levels f1− f3, m1−m3, and m8. Units: bond length A−B in Å; bond angle A−B−C in deg; dihedral angle A−B−C−D in deg measured clockwise from A−B to C−D. Parameters are ordered as in the *Z*-matrix (ref 37). Nonbonded values are enclosed in parentheses.

Table 3. Selected Physical Properties for Protonated Glycine Structures Calculated at the HF/6-311+G** and MP2/6-311+G** Optimized Levels[a]

property	$GlyH^+$(O)	$GlyH^+$(TS)	$GlyH^+$(N*)	$GlyH^+$(N)
	At the HF/6-311+G** Optimized Level			
E_e	−283.259556	−283.250913	−283.277719	−283.278526
E_{ZP}	62.67	60.59	63.55	63.69
$E - E_0$	3.24	2.85	2.94	3.49
S	72.26	69.62	70.49	75.90
$Q \times 10^{-13}$	0.9608	0.4927	0.6532	3.9397
$\nu^{\ddagger}$		1510.18 *i*	119.00 *i*	
	At the MP2/6-311+G** Optimized Level			
E_e	−284.184750	−284.177719	−284.233184	
E_{ZP}	58.71	58.45	59.90	
$E - E_0$	3.61	3.29	3.56	
S	75.71	73.59	75.08	
$Q \times 10^{-13}$	2.9061	1.7139	2.3290	
$\nu^{\ddagger}$		377.33 *i*		

[a] Temperatures: E_e, E_{ZP}, E_0, and $\nu^{\ddagger}$ at 0 K; E, S, and Q at 298.15 K. Units: E_e in hartrees; E_{ZP} and $E - E_0$ in kcal/mol; S in cal/K·mol; $\nu^{\ddagger}$ in cm^{-1}. See Tables S1 and S3 for properties of levels f1−f3 and m1−m3.

with a significantly smaller GB for formamide (ca. 175 kcal/mol for N-protonation) than ethyl amine (210.0 kcal/mol).[45] In fact, **6** and **8** are now calculated to be stable at the MP2/6-31G* level [Appendix A2]. In other words, structures resulting from O-protonation at either terminus of a peptide like **6** and **8** are relatively more stable than that of a protonated amino acid $H_2NCHRC(OH)_2^+$ like **2**.

In this work we study the MEP for the HF pair **1**/**2** as a model for the protonated termini of peptides, despite the instability of **2** in the gas phase. On the other hand, the MEP for the MP2 pair **3**/**4** serves a model for the protonated amino acids. Results and discussion concerning the proton transfers described by these two MEPs are presented below.

RESULTS

For a systematic study of the effect of basis functions on calculated structures, the 6-31G*, 6-31G**, 6-31+G**, and 6-311+G** sets were selected to show a gradual progression in the number and composition of basis functions. To investigate the effect of electron correlation, each basis set was used for both HF and MP2 optimizations. The resulting HF and MP2 structures for the reactant, TS or TS intermediates, and product associated with the proton transfer reaction are represented in Figures 2 and 3. Calculated data from all geometry optimizations (geometry and E_e) and frequency calculations (E_{ZP}, $E - E_0$, S, Q, and $\nu^{\ddagger}$) are presented in Tables 1−3 and S1−S3. Generally, those from the largest set 6-311+G** are listed explicitly in Figures 2 and 3 and Tables 1−3 as the best values, while those of the smaller sets are placed in Table S1−S3 of Supporting Information for reference. Other pertinent results are included in the Appendix.

The influence of polarization functions and correlation levels on relative energies are furthered examined by SP calculations with the 6-31+G(2d,2p) and 6-311+G(3df,2p) sets and the MP4 method. Alternative approaches such as the cc-pVDZ, aug-cc-pVDZ, and cc-pVTZ sets and the CCSD and DFT (B3LYP) methods are also tested. Results are included in Tables 1 and S1.

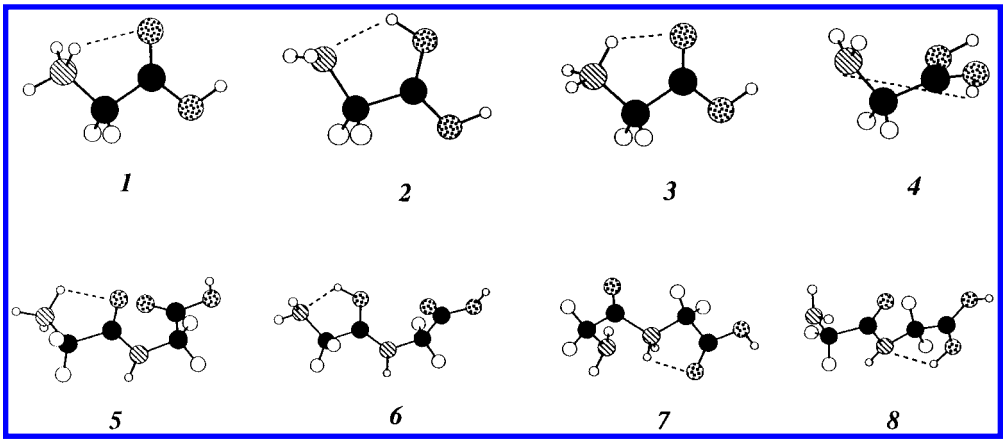

Figure 1. Structures associated with proton transfers in protonated glycine (top row) and diglycine (bottom row). The origin and destination of each proton transfer are connected by a dashed line. The atom patterns are C black, N striped, O patchy, and H blank.

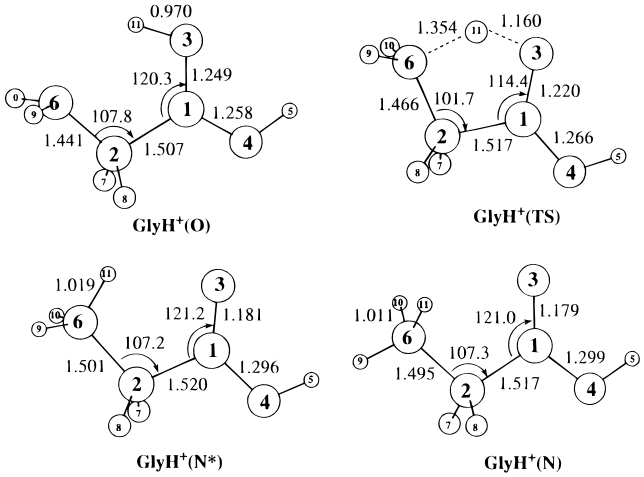

Figure 2. HF/6-311+G** structures associated with the proton transfer reaction in protonated glycine.

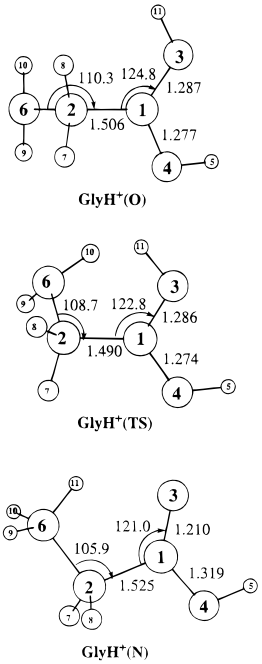

Figure 3. MP2/6-311+G** structures associated with the proton transfer reaction in protonated glycine.

The potential energy curves (PECs), accompanied by changes of key geometrical parameters during proton transfer, are shown in Figures 4 and 5 for HF/6-31G* and Figures 6 and 7 for MP2/6-31G*. Optimized parameters for the critical points on the HF and MP2 PECs are shown in Tables S4 and S5; E_e and parameters for each optimized point on the MP2 forward and reverse reaction paths are listed in Tables S6 and S7, and an analysis of the MP2 PEC is summarized in Tables 4 and S8. Tables S4−S8 are part of Supporting Information. The HF and MP2 PECs derived from larger basis sets 6-31G**, 6-31+G**, and 6-311+G** are expected to be comparable in shape and characteristics to those of the respective HF/6-31G* and MP2/6-31G* PECs [cf. Appendix A1].

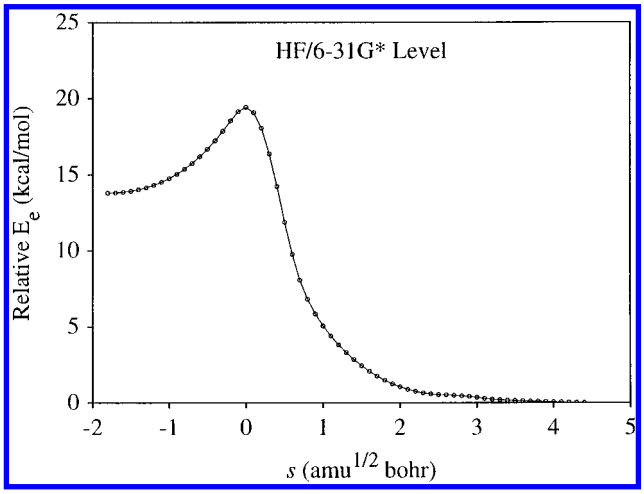

Figure 4. HF/6-31G* potential energy curve versus reaction coordinate s for the proton transfer reaction in protonated glycine.

For the proton transfer reaction at 298.15 K, changes in standard thermodynamic functions ($\Delta H°$, $\Delta S°$, $\Delta G°$, and K_p) and kinetic properties for the forward and reverse directions ($\Delta E^{\ddagger}_{0,f}$, κ_f, k_f, $\Delta E^{\ddagger}_{0,r}$, κ_r, and k_r) calculated from all four bases selected for the HF and MP2 optimizations are provided in Table 5. Temperature dependence of the thermodynamic and kinetic properties at the HF/6-31G* level is illustrated in Figure S1 of Supporting Information.

ELECTRONIC STRUCTURES

A. HF Optimizations. Geometrical parameters for the reactant GlyH$^+$(O), transition state GlyH$^+$(TS), intermediate species GlyH$^+$(N*), and product GlyH$^+$(N) from HF optimizations using the 6-31G*, 6-31G**, 6-31+G**, and 6-311+G** basis sets are found to be in good agreement

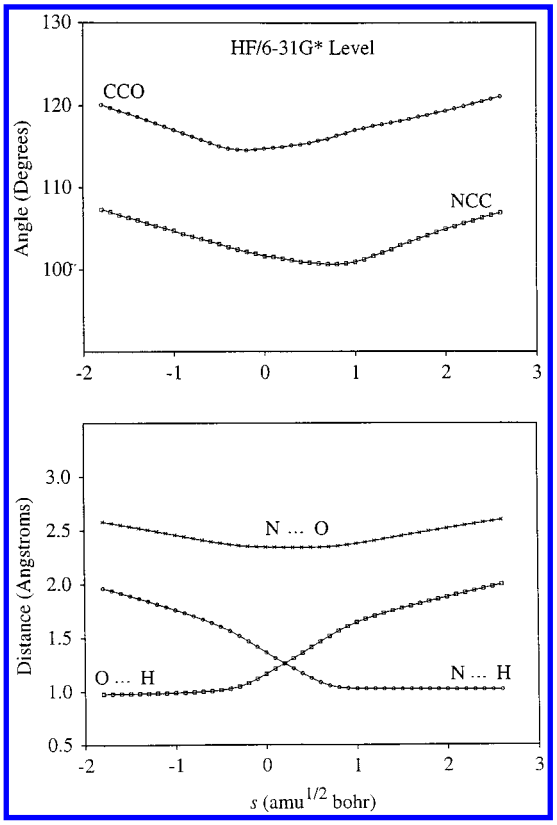

Figure 5. HF/6-31G* geometrical parameters versus reaction coordinate *s* for the proton transfer reaction in protonated glycine: bond angles CCO and NCC (top); interatomic distances O···H, N···H, and N···O (bottom).

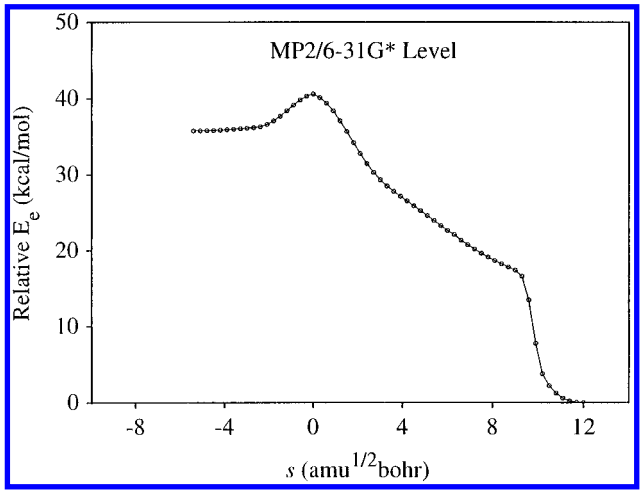

Figure 6. MP2/6-31G* potential energy curve versus reaction coordinate *s* for the proton transfer reaction in protonated glycine.

with one another (Tables S2 and 2). All four structures are symmetric (C_s) with respect to the plane containing the heavy atoms C1, C2, O3, O4, and N6; those for the reactant and product were known[19] and discussed[31] previously. Here we focus on the transition state and intermediate using the HF/6-311+G** values in Table 2 and Figure 2.

$GlyH^+$(TS) corresponds to the proton transfer barrier; it is a molecular complex containing a very strained five-membered ring structure H11−N6−C2−C1−O3 closed by N6···H11···O3 where H11 is the migrating proton (Figure 2). The short distances for N6···H11 (1.354 Å) and O3···H11 (1.160 Å) and the small angles for C2−N6···H11

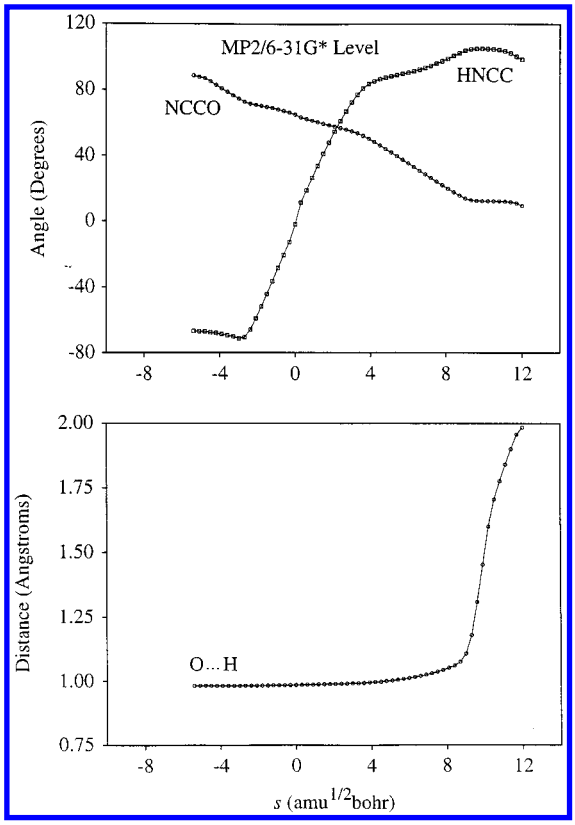

Figure 7. MP2/6-31G* geometrical parameters versus reaction coordinate *s* for the proton transfer reaction in protonated glycine: dihedral angles NCCO and HNCC (top); interatomic distance O···H (bottom).

angle (90.1°) and C1−O3···H11 (96.8°) imply that H11 is tightly held to N6 and O3 and the strong nonbonded hydrogen attraction may be the cause for the high ring strain. Other measures of the strain include the noticeably smaller C1−C2−N6 and C2−C1−O3 angles (101.7° and 114.4°) than those in the reactant and product. Note that the TS structure resembles the reactant more than the product (cf. the O3···H11 and C1−O3 distances) in accord with Hammond's rule.[46] $GlyH^+$(TS) is therefore formed early in the transfer process.

The structure residing at the end of the IRC path, $GlyH^+$(N*), is found to possess one imaginary vibrational frequency. An additional IRC calculation at the HF/6-31G* level reveals that $GlyH^+$(N*) links to $GlyH^+$(N) and its mirror image conformer through approximately ±60° rotations with respect to the H11−N6−C2−C1 torsional angle. Thus, $GlyH^+$(N*) is the internal rotational barrier for conformers arising from 3-fold rotations about the C2−N6 bond. We call $GlyH^+$(N*) an intermediate because its presence is necessary for reaching the final stable product. In view of the small changes in energy and geometry from $GlyH^+$(N*) to $GlyH^+$(N) (Tables 1 and 2), the IRC is taken to be continuous from the TS through the intermediate ($s = 2.1$ in Figure 4) to the product in order to simplify the kinetics calculations.

With respect to the electronic energy relative to $GlyH^+$(N), ΔE_e, we first review those from HF optimizations (f1−f4 in Table 1). Expanding 6-31G* to 6-31G** lowers the relative energies by about 3 kcal/mol for $GlyH^+$(O) and $GlyH^+$(TS) and 0.2 kcal/mol for $GlyH^+$(N*); however,

Table 4. Geometrical Parameters and Relative Electronic Energies of Selected Optimized Points on the MP2/6-31G* PEC Calculated at Different Levels[a,b]

		GlyH$^+$(O)	GlyH$^+$(TS)	P27	P32	GlyH$^+$(N)
path *s* (MP2)		−5.5	0.0	7.8	9.3	12.0
path *s* ("new")				−1.5	0.0	2.7
parameters:	NCCO	93	65	22	13	8
	HNCC	−66	−2	97	105	100
	O···H	0.984	0.986	1.044	1.180	1.980
	N···H	3.325	2.821	1.767	1.444	1.042
ΔE_e:	HF/6-31G*	28.47	33.03	16.20	19.89	0.00
	MP2/6-31G*	35.74	40.59	19.12	16.61	0.00
	CCSD/6-31G*	33.30	37.91	17.87	17.38	0.00
	(CCSD T1 diag)	(0.016)	(0.015)	(0.015)	(0.015)	(0.015)
	HF/6-31+G**	25.49	29.92	14.47	17.85	0.00
	MP2/6-31+G**	32.06	36.67	17.23	14.87	0.00
	B3LYP/6-311+G**	26.91	32.22	13.90	12.38	0.00

[a] Units: *s* in amu$^{1/2}$ bohr; angles in deg; distance in Å; ΔE_e in kcal/mol. Selected points include the three critical points [GlyH$^+$(O), GlyH$^+$(TS), and GlyH$^+$(N)] and two optimized points (P27 and P32) on the MP2/6-31G* IRC of Figure 6 (cf. Tables S5−S8). Path *s* (MP2) is the calculated MP2/6-31G* IRC; path *s* ("new") is a hypothetical path with P27 and GlyH$^+$(N) as minima and P32 as the transition state. [b] Parameters and ΔE_e refer to the MP2/6-31G* optimized geometries in Tables S5 and S6. Parameters include dihedral angles NCCO and HNCC and interatomic distances O···H and N···H (cf. Figures 7 and 8). See footnote *c* of Table 1.

Table 5. Thermodynamic and Kinetic Properties for the Reaction GlyH$^+$(O) ⇌ GlyH$^+$(N) at 298.15 K Calculated at Different HF and MP2 Optimized Levels[a]

property	6-31G*	6-31G**	6-31+G**	6-311+G**
		At the HF Optimized Levels		
$\Delta H°$	−12.41	−9.93	−10.27	−10.63
$\Delta S°$	2.88	4.94	4.27	3.64
$\Delta G°$	−13.27	−11.40	−11.54	−11.72
K_p	5.33×10^9	2.27×10^8	2.88×10^8	3.90×10^8
$\Delta E^{\ddagger}_{0,f}$	3.47	3.01	3.38	3.35
κ_f	3.84	3.60	3.60	3.60
k_f	3.72×10^{10}	7.53×10^{10}	3.92×10^{10}	4.02×10^{10}
$\Delta E^{\ddagger}_{0,r}$	16.12	13.23	13.92	14.23
κ_r	3.52	3.27	3.31	3.31
k_r	6.44	2.97×10^2	1.25×10^2	9.53×10^1
		At the MP2 Optimized Levels		
$\Delta H°$	−34.26	−31.42	−30.70	−29.25
$\Delta S°$	−0.08	0.28	−0.85	−0.63
$\Delta G°$	−34.24	−31.50	−30.45	−29.06
K_p	1.25×10^{25}	1.23×10^{23}	2.09×10^{22}	2.00×10^{21}
$\Delta E^{\ddagger}_{0,f}$	4.69	4.69	4.47	4.15
κ_f	1.17	1.17	1.16	1.16
k_f	1.74×10^9	1.80×10^9	2.24×10^9	3.85×10^9
$\Delta E^{\ddagger}_{0,r}$	38.88	36.04	35.06	33.35
κ_r	1.15	1.15	1.14	1.14
k_r	1.38×10^{-16}	1.45×10^{-14}	1.06×10^{-13}	1.87×10^{-12}

[a] Units: $\Delta H°$ and $\Delta G°$ in kcal/mol; $\Delta S°$ in cal/mol·K; k_f and k_r in s^{-1}. $\Delta H°$, $\Delta S°$, $\Delta G°$, κ_f, and k_f are for the forward reaction; κ_r and k_r are for the reverse reaction; and K_p is for the equilibrium. Physical properties in Tables 1, 3, and S3 are used for these calculations at the respective optimized levels.

successive expansions from 6-31G** to 6-31+G** and 6-311+G** show only small incremental increases. These results imply that adding hydrogen p polarization functions to 6-31G* to form 6-31G** strengthens the bonded and nonbonded interactions O−H, N···H−O, and N···H···O more than N−H and N−H···O because oxygen is more electronegative than nitrogen, but balancing 6-31G** with non-hydrogen sp diffuse functions to form 6-31+G** and enhancing 6-31+G** with a third set of split-valence functions to form 6-311+G** lead to finer adjustments in relative energy. The suggested changes are consistent with changes of the bonded and nonbonded distances H11−O3, H11···N6, H11−N6, and H11···O3 in Tables S2 and 2.

We next investigate changes of ΔE_e brought by electron correlation (MP2 or MP4) on HF structures with the same basis set. At the HF/6-31+G** geometries, MP2/6-31+G** produces an increase of 4 kcal/mol for GlyH$^+$(O), a decrease of 5 kcal/mol for GlyH$^+$(TS), and a decrease of 0.5 kcal/mol for GlyH$^+$(N*) from the HF/6-31+G** values (f3 and f5 of Table 1). Comparable changes are seen from HF/6-31G* to MP2/6-31G* at the HF/6-31G* geometries (Table 1). These large and erratic changes of energies suggest that direct MP2 geometry optimizations may yield a totally different set of structures—this is indeed the case confirmed by subsequent MP2 optimizations. Finally, we observe that increasing the correlation order from MP2 to MP4 has a relatively small effect; for example, the maximum change in ΔE_e is an increase of 0.6 kcal/mol for GlyH$^+$(TS) on going from MP2/6-31+G** to MP4/6-31+G** at the HF/6-31+G** geometries (f5 and f6 of Table 1).

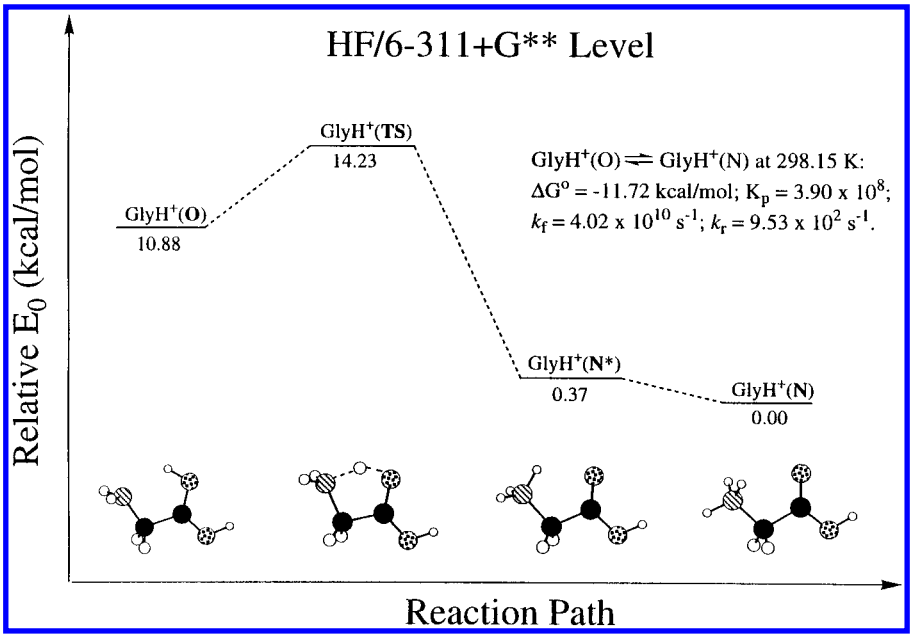

Figure 8. HF/6-311+G** structures and thermodynamic and kinetic properties associated with the proton transfer reaction in protonated glycine.

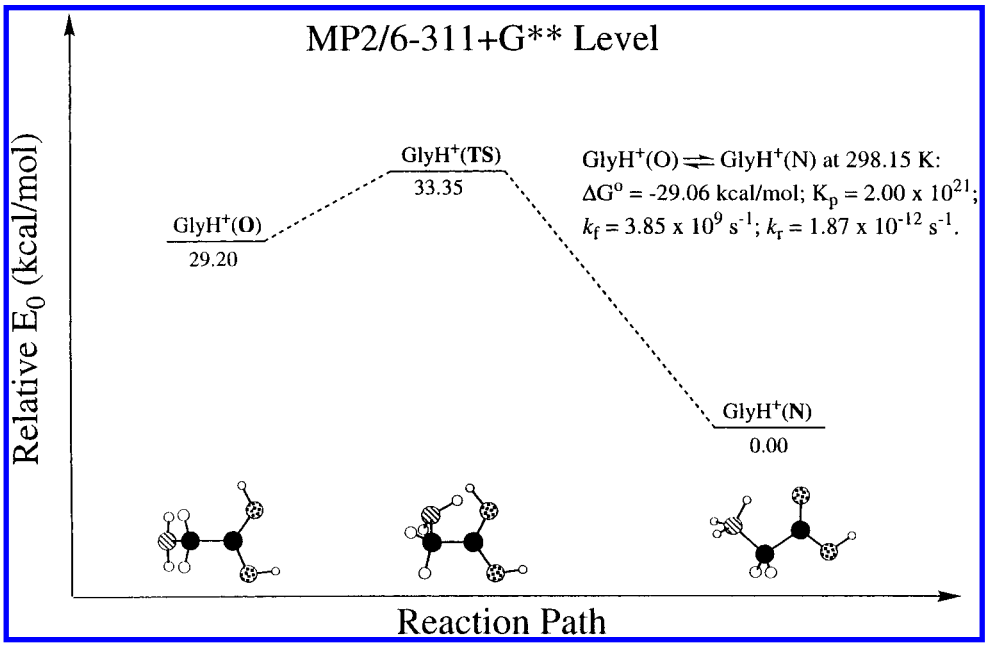

Figure 9. MP2/6-311+G** structures and thermodynamic and kinetic properties associated with the proton transfer reaction in protonated glycine.

Critical to the kinetics study is the barrier height for the proton transfer reaction [$E_0^{\ddagger}$ of eq 10 and Table 4]. With regard to the basis effect, consider the levels representing the smallest and largest basis sets, HF/6-31G* and HF/6-311+G**. The respective barriers are 3.47 and 3.35 kcal/mol for the forward reaction 1 and 16.12 and 14.23 kcal/mol for the reverse reaction 2. These results indicate that $E_0^{\ddagger}$ is nearly independent of the basis size for the forward reaction but is affected by the presence of hydrogen polarization functions (and non-hydrogen diffuse functions to a lesser degree) for the reverse reaction. Thus the 6-31G* basis underestimates the reverse barrier by about 2 kcal/mol.

The correlation effect on barrier height is truly significant (Table 1). Before correlation, the TS is the barrier that lies above the reactant, intermediate, and product in energy (f1−f4). But after including the MP2, MP4, or B3LYP correlation contribution (f5−f10), the TS falls below the reactant by 2−3 kcal/mol. As a consequence, the forward reaction from $GlyH^+$(O) to $GlyH^+$(N*) is reduced to a barrierless process, and $GlyH^+$(O) is expected to vanish into $GlyH^+$(N*). Furthermore, $GlyH^+$(N*) now lies 0.1−0.6 kcal/mol below $GlyH^+$(N) to become the most stable N-protonated species. These findings suggest that the HF species in Figure 2, with $GlyH^+$(N*) as the only exception, are unstable in the gas phase (vide supra).

B. MP2 Optimizations. The MP2 geometries for $GlyH^+$(O), $GlyH^+$(TS), and $GlyH^+$(N) calculated from the four selected basis sets are again fairly similar (Tables S2 and 2). The only prominent difference concerns the position of the ammonium hydrogens relative to the carbonyl oxygen in the global minimum $GlyH^+$(N) where the ionic H-bond N−H···O is present. As the basis expands, 6-31G* →

6-31+G** → 6-311+G**, the nonbonded distance H11···O3 increases, 1.980 Å → 2.054 Å → 2.075 Å, showing an increase in the vicinal steric repulsion (VSR) between $-NH_3^+$ and −C2(C1)(H7)(H8) relative to the hydrogen bonding attraction (HBA) of N−H···O. (Note the H11···O3 distance of 6-31G** is 1.937 Å because of an "imbalance" in the basis.[31,47,48]) The relative strengths of the opposing VSR and HBA forces in a MP2 correlated structure appear to depend sensitively on the basis composition and size.[31]

We now focus on the three MP2/6-311+G** structures $GlyH^+$(O), $GlyH^+$(TS), and $GlyH^+$(N) in Table 2 and Figure 3, which are identified as the asymmetric structures 6m, 8t, and 1m in a preceding study[31] [cf. Appendix A3]. To illustrate the conformation of the ammonium terminus, values of the dihedral angles N6−C2−C1−O3 (ψ_2) and H10−N6−C2−C1 (ψ_1) in Table 2 are used. The 6m structure, like the other MP2 O-protonated species, has no hydrogen bonding attraction between the $-NH_2$ group and the charged $-C(OH)_2^+$ fragment; in fact, the N6−C2 bond is orthogonal to the O3−C1 bond ($\psi_2 = 95°$), and the two amino hydrogens are about equally displaced from the C2−C1 bond ($\psi_1 = -66°$). To reach the transition state 8t, 6m undergoes rotation about the C−C bond for O3 to approach N6 (at $\psi_2 = 70°$) and rotation about the C−N bond to move the amino hydrogen atoms away from H11 to make room for H11 to migrate (at $\psi_1 = -1°$). Note that 8t is not a molecular complex, N···H···O (TS), but a "normal" TS of the O-protonated species, N···H−O (TS). Finally, the proton migrates and forms the product 1m (at $\psi_2 = 11°$ and $\psi_1 = 87°$) with an ionic H-bond N−H···O at a H11···O3 distance of 2.075 Å. To accomplish the proton transfer we note that changes in ψ_2 (95° → 70° → 11°) and ψ_1 (−66° → −1° → 87°) are physically reasonable. It should be pointed out that the proton transfer path commencing at 6m is the only MP2 path discovered after an extensive search over possible paths involving O-protonated conformers of lower energy (4m and 5m).[27,31] Geometrically, 6m ($\psi_2 = 95°$) is closer to 1m ($\psi_2 = 11°$) than 4m ($\psi_2 = 185°$) and 5m ($\psi_2 = 180°$) with respect to rotation around the C−C bond and thus has a shorter route for the proton transfer. Furthermore, no O-protonated minimum ($\psi_2 < 95°$) has been found thus far that is closer to 1m than 6m.[31]

Correlation effect on the calculated structures of $GlyH^+$ is drastic, demonstrated by the two entirely different sets resulting from HF and MP2 optimizations (Figures 2 and 3). The reason is an underestimation of internal hydrogen attraction involving the highly electronegative oxygen and nitrogen atoms by the HF method. A discrepancy between the HF and MP2 structures for the Gly conformers was first noted by Frey et al.;[18] we found the correlation effect enhanced in the case of $GlyH^+$ because of the added H^+.[31] For the $GlyH^+$ species involved in this investigation, the following discrepancies are noted. First, the HF reactant and TS do not remotely resemble any minima or saddle points on the MP2 PES. This is attributed to the MP2 prescription of a relatively strong ionic N···H attraction in the N···H···O arrangement that spontaneously relaxes to form N−H···O. Second, the HF intermediate and product resemble conformationally to two MP2 transition states (1n and 1t) close in energy to the global minimum (1m). Finally, the MP2 reactant and TS do not remotely resemble any minima or saddle points on the HF PES. [Counter examples are protonated formamide and diglycine documented in Appendixes A1 and A2.]

Values of ΔE_e from MP2 optimizations show $GlyH^+$(O) and $GlyH^+$(TS) decrease roughly by 3, 1, and 2 kcal/mol as the basis expands in the sequence 6-31G* → 6-31G** → 6-31+G** → 6-311+G** (m1−m4 in Table 1). Correlation enhancement MP2 → MP4 induces a small decrease of 0.4 kcal/mol at the MP2/6-311+G** geometries (m4 and m5). These trends are quite similar to those deduced from HF optimizations, and hence the explanations given earlier apply here. The big difference between the HF and MP2 values is the magnitude of ΔE_e: The MP values are around 15−20 kcal/mol higher than the corresponding HF values due to the absence of the strongly attractive N···H−O and N···H···O arrangements in the MP2 structures for $GlyH^+$(O) and $GlyH^+$(TS).

The barriers for proton transfer ($\Delta E_0^{\ddagger}$) at the MP2/6-31G* and MP2/6-311+G** levels are computed to be 4.69 and 4.15 kcal/mol for the forward direction and 38.88 and 35.35 for the reverse direction (Table 5). Compared with the corresponding HF values, the barrier heights are about 1 kcal/mol higher for the forward direction but 20 kcal/mol higher for the reverse direction. Again, the large reverse barrier is due to the absence of the N···H···O arrangement in the MP2 structure for $GlyH^+$(TS).

C. Additional Calculations. To circumvent the cost of a benchmark calculation for the GB of glycine,[29] we adopted a composite procedure similar to the G2(MP2) theory of Pople and co-workers to attain high-level accuracy from low-level computations.[49] The procedure generates the E_e at level "L2"//L1, where "L2" is a composite level for energy and L1 is for geometry at a lower level (cf. f8 and m7 of Table 1). We found that the calculated GB (Gly) converged to 203.5 kcal/mol at level "MP4/6-31+G(2d,2p)"//MP2/6-31+G** (*x*) and remained unchanged at the higher level "MP4/6-311+G-(3df,2p)"//MP2/6-311+G** (*y*):[29] the calculated GB is in excellent agreement with the experimental value 203.7 kcal/mol.[45] Thus *x* and *y* may be taken respectively as levels that yield "near" and "true" limiting values in accuracy.

For the HF species in Figure 2, the composite level "MP4/6-31+G(2d,2p)" at the HF/6-31+G** geometries (f8) yields a negative E_e barrier for the forward reaction, $GlyH^+$(O) → $GlyH^+$(TS), i.e., $\Delta E_{0,f}^{\ddagger} = -2.41$ kcal/mol. But the same "L2" at the MP2/6-31+G** geometries (*x*) was shown previously to be highly accurate in the GB calculation. Thus the negative barrier resulting from f8 provides the definitive evidence that the HF geometries for $GlyH^+$(O) and $GlyH^+$-(TS) are unstable in the gas phase (*vide supra*). For the MP2 species in Figure 3, the composite level "MP4/6-311+G-(3df,2p)" at the MP2/6-311+G** geometries (m7, same as *y*) yields E_e barriers for the forward and reverse reactions as 4.47 and 33.23 kcal/mol, which compare well with the MP2/6-311+G** optimized (m4) barriers 4.41 and 34.80 kcal/mol. Since a property derived from m7 virtually reaches the convergence limit for accuracy, the closeness between the barrier heights of m7 and m4 ensures that the MP2/6-311+G** optimized level (m4) is sufficiently accurate for the study of proton transfer reaction.

In view of the drastically different HF and MP2 structures for $GlyH^+$(O) and $GlyH^+$(TS) a question is raised on the

adequacy of the present single-reference electron correlation procedure. To look for the possibility of substantial multireference character being present at the four HF and three MP2 extrema, CCSD/6-31G* electronic energies and T1 diagnostics were calculated at the respective HF/6-31G* and MP2/6-31G* optimized geometries (Tables S4 and S5).[50,51] For the HF extrema (Table 1) the resulting CCSD ΔE_e exhibit good convergence behavior in the sequence MP2 → MP3 → CCSD → MP4, and the CCSD T1, 0.013−0.014, are below the recommended value of 0.020 for a multireference treatment. Similar results are deduced for the MP2 extrema (Table 4). These CCSD tests verify that the MP perturbation expansion is converging fairly rapidly from MP2 to MP4.

Two alternatives[39,40] to the more traditional ab initio approaches[36] are explored for their potential use in proton transfer studies. Their applications on $GlyH^+$ (f9, f10, and m8−m10) complement previous applications on Gly by Hu et al.[22] and Baron et al.[25] and provide documentation on their applicability to studies of gas-phase ion chemistry.

The Dunning augmented correlation-consistent (cc) sets were shown by Del Bene[52] to yield highly accurate proton affinities (PAs) in small molecules. Recently we demonstrated that the PA of methyl amine calculated at the CCSD(T)/aug-cc-pVTZ level fell within 0.5 kcal/mol of the experimental value.[29] Constrained by the larger size of $GlyH^+$, the cc bases employed here are limited to double- and triple-ζ functions. First consider the MP2 structures. The present study finds MP2/cc-pVDZ optimizations (m8) with 100 basis functions (bfs) yielding quite similar geometrical parameters as the MP2/6-31+G** optimizations (m3) with 125 bfs. But the cc m8 is more efficient than the standard m3 in reducing the ΔE_e of $GlyH^+$(O) and $GlyH^+$(TS) to reach the lower limiting values exemplified by m7. These comparisons suggest that the cc bases are more efficient or balanced than the comparable standard bases at the double-ζ level. At the triple-ζ level, the ΔE_e values from SP calculations at levels MP2/cc-pVTZ (m9) with 234 bfs and MP2/6-311+G(3df,2p) (m6) with 249 bfs are very similar and close to the limiting values. Next consider the HF structures. The same observation holds: Level MP2/aug-cc-pVDZ (f9) with 169 bfs is more effective than level MP2/6-31+G(2d,-2p) (f7) with 173 bfs in reducing the ΔE_e of $GlyH^+$(O) and $GlyH^+$(TS). Better accuracy is achieved with fewer bfs when the cc bases are used instead of the standard bases at the double-ζ level.

In recent years DFT has become increasingly popular for two major reasons: (a) DFT gives more reliable results than HF by virtue of its partial inclusion of electron correlation, and (b) the cost of computations on large molecules or large number of data points is significantly lower for DFT than MP2. The second reason has propelled the use of DFT PES in kinetics calculations.[53] We found the DFT GB of Gly to be quite satisfactory.[29] Present B3LYP/6-311+G** calculations on the barriers of proton transfer reaction in $GlyH^+$ reveal the following: (a) DFT correctly contradicts the HF prediction of a barrier in the transfer path (f10 vs f4), and (b) DFT yields noticeably lower barrier for the reverse direction than MP2 (ca. 3 kcal/mol from m10 vs m4). While (a) represents a triumph for DFT as regards reliability in qualitative predictions, (b) leaves room for future improvement in quantitative assessments.

PROTON TRANSFER MECHANISMS

The HF/6-31G* potential energy curve is plotted against the reaction coordinate *s* in Figure 4. The curve begins at the $GlyH^+$(O) ($s = -1.8$) on the left, rises to a maximum at $GlyH^+$(TS) ($s = 0$), and ends at $GlyH^+$(N) ($s > 2.7$) on the right. Note the PEC slopes gently upward before the TS and falls very steeply after the TS. The intermediate $GlyH^+$(N*) ($s = 2.1$) is the end point for proton transfer, and the curve following $s > 2.1$ corresponds to internal rotation around the C−N bond to reach $GlyH^+$(N).

Geometrical parameters crucial to an understanding of different atom movements during proton transfer are plotted against *s* in Figure 5. It can be seen that the extent of hydrogen (H11) migration is tied to the O−H or N−H bond formation (bottom figure). Starting from the TS, the formation of the O−H bond in the reverse direction is slightly faster than the formation of the N−H bond in the forward direction: the O−H bond is about 96% complete at $s = -0.5$, while the N−H bond is 89% complete at the comparable $s = 0.5$. Changes in the N···O distance and NCC and CCO angles along *s* (top figure) provide valuable clues to the extent of nitrogen (N6) and oxygen (O3) participation in the proton transfer process. The N···O distance displays a smooth decrease along *s* as the reaction goes from either direction to the TS. If we consider proceeding forward from $s = -1.8$ to $s \leq -0.5$, the O···H bond shows almost no change, while the N···O distance and the CCO angle both decrease noticeably. Similar situation occurs on going in the reverse direction from $s = 2.7$ to $s \geq 0.75$ with regard to the N−H bond, the N···O distance, and the NCC angle. Based on these observations, we conclude that the hydrogen (H11) migration takes place mainly in the region $-0.5 < s < 0.75$, and heavy-atom movements (principally those of O3 and N6) feature prominently outside this region.

The MP2/6-31G* potential energy curve is plotted in Figure 6. To monitor the proton migration, changes of three key geometrical parameters (the O···H distance and NCCO and HNCC dihedral angles) along *s* are shown in Figure 7. It can be seen that when $s < 9$, the O···H distance is nearly constant, which implies that there is essentially no proton movement (bottom figure). In this region the only physical movement is internal rotations about the C−C and C−N bonds as depicted by changes in NCCO (ψ_2) and HNCC (ψ_1) (top figure). Therefore, the PEC for this region refers to coupled internal rotations. In the region $s > 9$ lies the migration of H11 from O3 to N6 in a molecular framework nearly static in all other internal motions: This is manifested in the nearly constant NCCO and HNCC, sharp rise in O···H, and marked drop of potential energy shown in Figures 6 and 7.

The HF PEC of Figure 4, *s* (HF), agrees with chemists' conception of proton transfer, whereas the MP2 PEC of Figure 6, *s* (MP2), seems unnatural because it shows internal rotations prior to proton transfer. Intuitively, one expects the extrema of a "true" transfer path, *s* ("true"), looking more like those of *s* (HF) than *s* (MP2). Despite the computational evidence to the contrary, we continued the search of *s* ("true") as follows. The goal is to find a new MP2 O-protonated minimum in closer proximity to the N-protonated species on the IRC and a new MP2 TS that resembles more like a molecular complex.

Geometries of selected optimized points on the *s* (HF) and *s* (MP2) paths were used for SP calculations at MP2/6-31+G**, a level higher than those cmployed for the original IRC derivations. For the HF/6-31G* path $GlyH^+$(O) → $GlyH^+$(TS), eight points on *s* (HF) from −1.8 to 0.0 (Table S4 and Figure 4) were chosen for MP2/6-31+G** SP calculations. The resulting ΔE_e decreases from 15.29 to 12.26 kcal/mol without revealing a new MP2 maximum for TS. For the MP2/6-31G* path $GlyH^+$(TS) → $GlyH^+$(N), MP2/6-31+G** SP calculations were performed at 15 points on *s* (MP2) from 0.0 to 12.0 (Figure 6), including the two end points (Table S5) and intermediate points P15−P19 and P24−P33 (Table S6). The resulting ΔE_e decreases from 36.67 to 0.00 kcal/mol, showing no new MP2 minimum and/or maximum. Yet, the HF/6-31G* and HF/6-31+G** SP values at the selected points suggest a shallow HF "minimum" at P27 for an O-protonated species and a HF "maximum" at P32 for a TS (Tables 4 and S8).

Geometry optimizations from selected points of *s* (HF) and *s* (MP2) were also carried out. Symmetry restricted (C_s) MP2/6-31G* optimizations starting from the symmetric HF/6-31G* $GlyH^+$(O) geometry converged to the symmetric MP2/6-31G* N-protonated structure 1n (cf. ref 31). MP2/6-31+G** optimization from the MP2/6-31G* geometry of P15 (at $s = 4.2$ and $\psi_2 = 48°$) converged to the MP2/6-31+G** structure of 1m. The two TS optimizations, (1) symmetry restricted MP2/6-31G* optimization from the symmetric HF/6-31G* $GlyH^+$(TS) geometry and (2) MP2/6-31+G** optimization from the MP2/6-31G* P32 geometry, either blew up or showed no sign of convergence. To summarize, all optimizations failed to identify a new MP2 minimum and/or a new MP2 TS in this region of MP2 IRC ($0 < s < 12$).

The route connecting the five points on *s* (MP2), $GlyH^+$(O) → $GlyH^+$(TS) → P27 → P32 → $GlyH^+$(N), are characterized in Table 4 by geometrical parameters NCCO, HNCC, O···H, and N···H that reflect coupled internal rotations and proton transfer (Figure 7) and by ΔE_e calculated from combinations of the HF, MP2, CCSD, and B3LYP methods and the 6-31G*, 6-31+G**, and 6-311+G** basis sets. The ΔE_e incorporating some level of electron correlation show extrema at the originally designated sites, $GlyH^+$(O), $GlyH^+$(TS), and $GlyH^+$(N), at *s* (MP2) = −5.5, 0.0, and 12.0. The ΔE_e at the HF level show a "new" path with extrema at P27, P32, and $GlyH^+$(N) which are now assigned as *s* ("new") = −1.5. 0.0, and 2.7. [Note: *s* ("new") is a hypothetical path and P27 and P32 are not real stationary points.] Extrema of *s* ("new") have conformations compatible to those at *s* (HF) = −1.8, 0.0, and 2.1 (Figure 2), but NCCO (ψ_2) of *s* ("new") varies from 22°, 13°, to 8° as compared with 0° for the corresponding symmetric structures on *s* (HF).

The above analysis reveals that the physical paths depicted for the *actual* proton transfer by *s* (HF) and *s* (MP2) are roughly similar. The *s* (HF) route from −1.8 to 2.1 for $GlyH^+$(O) → $GlyH^+$(TS) → $GlyH^+$(N*) is geographically similar to the *s* (MP2) route from 7.8 to 12.0 after the O-protonated species has undergone the necessary internal rotations for the transfer. The lack of a MP2 barrier around *s* (MP2) = 9.3, which corresponds to the HF barrier at *s* (HF) = 0, is due to a smoothly relaxing N6···H11···O3 arrangement in the MP2 prescription for the transit of H11.

To conclude, the search for a proton transfer path *s* ("true") that forgoes internal rotations failed at the present level of correlation theory. Yet, there seems to be a hidden path *s* ("new") with extrema resembling those of P27, P32, and $GlyH^+$(N) in Table 4 for the O-protonated, TS, and N-protonated species, respectively, which are conformationally compatible with the extrema depicted by *s* (HF). There remains the possibility that *s* ("true") would emerge if geometry optimizations were carried out at a very high level of correlation theory[54] with a nearly complete basis set [e.g., CCSD(T)/aug-cc-pVTZ]. Needless to say, such optimizations are not feasible at present.[29] The CCSD/6-31G* and B3LYP/6-311+G** SP calculations at the selected points of *s* (MP2) in Table 4 further suggest that the PEC ("true") in the region between P27 and P32 would be nearly flat. As a result, the physical existence of *s* ("true") would be elusive at best.

THERMODYNAMICS AND KINETICS

The physical properties associated with the nuclear motion (translations, rotations, and vibrations) in the relevant $GlyH^+$ species remain nearly constant with respect to basis change at either the HF or MP2 level (Tables S3 and 3). Calculated frequencies and zero-point energies are not scaled[31] for eqs 4−6 in order to be consistent with the harmonic vibrational model employed for eqs 9−11. For the forward reaction 1 at 298.15 K, the ΔE_{ZP}, $\Delta(E - E_0)$, and $-T\Delta S$ terms are one to two orders of magnitude smaller than the electronic term ΔE_e because the reactant and product are both isomers of protonated glycine. For example, ΔE_e, ΔE_{ZP}, $\Delta(E - E_0)$, and $-T\Delta S$ at the MP2/6-311+G** level are −30.39, 1.19, −0.05, and 0.19 kcal/mol, respectively (cf. Table 3).

The thermodynamic properties for the reaction at 298.15 K are shown in Table 5. $\Delta H°$ is negative, indicating an exothermic reaction. The $\Delta H°$ values from MP2 optimizations are significantly more negative (ca. 20 kcal/mol) than those from HF optimizations because of the obviously different electronic structures (and hence ΔE_e) for the relevant species. The $\Delta S°$ values are very small (below 5 cal mol^{-1} K^{-1}), due in part to the structural similarity between isomeric species. Since the small $\Delta S°$ makes a negligible contribution, $\Delta G°$ is essentially determined by $\Delta H°$. At equilibrium, the product fully dominates the population as K_p is uniformly large.

The rate constants for proton transfer in the forward and reverse directions, k_f and k_r, corrected for tunneling by κ_f and κ_r in eq 12, are also shown in Table 5. Around room temperature, the transfer process in the forward direction is much more rapid than in the reverse direction, especially at the MP2 level. The k_f and k_r are, respectively, on the order of 10^{10} and 10^2 at HF/6-311+G** and 10^9 and 10^{-12} at MP2/6-311+G**. Tunneling appears prominent for HF ($\kappa \sim 4$) and is insignificant with MP2 ($\kappa \sim 1$). These differences in k and κ between the HF and MP2 values may be explained satisfactorily by differences in $E_0^{\ddagger}$ and $\nu^{\ddagger}$ as the ratio $Q^{\ddagger}/Q^R$ is nearly the same.

Temperature changes for the thermodynamic properties are shown in Figure S1 for the HF/6-31G* level. (Higher level frequency calculations are too costly.) Although the HF values for $\Delta H°$, $\Delta G°$, and K_p are substantially smaller than the MP2 values because of a smaller ΔE_e, the temperature dependent terms such as $\Delta(E - E_0)$ and $-T\Delta S$ are

expected to be comparable (cf. values for 298.15 K in Tables S3 and 3). Thus we expect that the MP2 plots roughly resemble the HF plots in Figure S1 after a change in the vertical scale to allow for a larger initial magnitude from a larger ΔE_e. Likewise, the HF curves for ln k versus T may be translated to comparable MP2 curves by only considering the difference incurred by $-E_0^{\ddagger}/(k_B T)$ in eq 9 since the contribution of [ln κ + ln $(Q^{\ddagger}/Q^R)$] is small.

The HF/6-31G* results for temperature changes bring out interesting trends. Both $\Delta H°$ and $\Delta S°$ rise from 100 K to a maximum around 300 K and then gradually decrease with increasing temperature. On the basis of the curvatures of the plots, it seems fairly certain that $\Delta H°$ is negative and $\Delta S°$ is positive at any temperature above 0 K. As temperature rises, $\Delta G°$ decreases monotonically while ln K_p drops dramatically at first and then drifts toward a constant over 1000 K. We conclude that the proton transfer reaction is thermodynamically spontaneous at any temperature. As for the rate constants, ln k_f and ln k_r show the expected decrease when temperature is lowered. At temperatures less than 500 K, where the forward reaction clearly dominates the proton transfer process, lowering the temperature produces a much more dramatic drop for the reverse rate than the forward rate.

SUMMARY

The minimum energy paths for intramolecular proton transfer in gaseous protonated glycine were approximated by intrinsic reaction coordinates calculated at the HF/6-31G* and MP2/6-31G* levels. The HF and MP2 levels of theory led to significantly different protonated structures associated with the transfer. After a conformational analysis relying on ab initio results and chemical evidence, the HF path is suggested as a model for peptides protonated at either terminus, while the MP2 path is proposed as a model for protonated amino acids.

The HF path (Figures 2 and 4) begins with the most stable O-protonated conformer $GlyH^+$(O), rises monotonically to form the molecular complex $GlyH^+$(TS) at the early stage of transfer, and falls monotonically to a N-protonated saddle point $GlyH^+$(N*) before converting to the global minimum $GlyH^+$(N). The MP2 path (Figures 3 and 6) starts with a $GlyH^+$(O) some 20 kcal/mol higher in energy than its HF counterpart, undergoes coupled internal rotations about the C−C and C−N bonds to form $GlyH^+$(TS) while remaining an O-protonated species, and continues the coupled rotations until the amino group is in a favorable orientation to accept the proton prior to disengaging the proton to form $GlyH^+$(N). The dissimilarity between the two paths may be attributed to the total absence in the MP2 stationary states two structural moieties: the ionic H-bond N···H−O [as in the HF structure for $GlyH^+$(O)] and the nonbonded ionic arrangement N···H···O [as in the HF structure for $GlyH^+$(TS)]. The enhanced hydrogen interactions among the N, H, and O atoms in these MP2 correlated structures lead to an ionic H-bond N−H···O exclusively [as in the MP2 structure for $GlyH^+$(N)]. Clearly, the marked differences between the HF and MP2 structures are consequences of including electron correlation in geometry optimizations of molecular systems such as glycine (ref 18) and protonated glycine (ref 31).

The HF/6-31G* and MP2/6-31G* structures for proton transfer in $GlyH^+$ were reoptimized with the 6-31G**, 6-31+G**, and 6-311+G** basis sets. Analyses are made to identify the effects of basis set and electron correlation on calculated structures. Generally, basis change has little effect on HF geometries but does influence the extent of ionic hydrogen bonding (N···H···O) in the MP2 structure for $GlyH^+$(N). As for energies, more reliable results are expected when hydrogen polarization functions are balanced by non-hydrogen diffuse functions (6-31G** vs 6-31+G**) and valence functions are increased from double to triple ζ (6-31+G** vs 6-311+G**).[47] Incorporating electron correlation into the HF structures $GlyH^+$(O) and $GlyH^+$(TS) yields drastically different relative energies (HF/6-31G* vs MP2/6-31G*), while MP4 single-point calculations lowers the MP2 relative energy of a given (HF or MP2) structure by a small amount (ca. 0.5 kcal/mol). Additional calculations using the larger bases 6-31+G(2d,2p) and 6-311+G(3df,-2p), the correlation-consistent bases cc-pVDZ, aug-cc-pVDZ, and cc-pVTZ and the DFT (B3LYP) method on selected HF and MP2 optimized geometries provide comparisons and documentation of importance to computational chemistry.

For the proton transfer reaction in the gas phase at 298.15 K and 1 atm, thermodynamic properties including enthalpy, entropy, Gibbs free energy, and equilibrium constant ($\Delta H°$, $\Delta S°$, $\Delta G°$, and K_p) were evaluated at all HF and MP2 optimized levels. The rate constants for the forward and reverse reactions (k_f and k_r) were estimated by means of the conventional transition state theory. A summary of the results obtained with the largest basis set selected for the HF and MP2 optimizations, HF/6-311+G** and MP2/6-311+G**, are shown schematically in Figures 8 and 9. These values indicate that the proton in a carbonyl O-protonated glycine undergoes a rapid migration to the amino nitrogen atom, while the reverse process is extremely unfavorable kinetically. This proton transfer process is thermodynamically spontaneous, leading to an equilibrium that consists almost entirely of the N-protonated glycine.

CONCLUDING REMARKS

Compared with previous model biological systems studied by the ab initio approach, the protonated glycine represents a larger and more realistic model. Because of the molecular size, the minimum energy path and rate constant for the proton transfer reaction are estimated using theoretical equations containing numerous approximations; on the other hand, the electronic structures involved in the transfer are determined to a high degree of rigor. We have reported the computational results from different theoretical levels for future references.

In this model study we have shown how MP2 structures are drastically different from the HF structures as a consequence of including electron correlation in geometry optimizations. Considering the likelihood of employing the HF method in future studies of proton transfer, our findings call attention to the possible errors that might arise from HF applications to molecular systems that contain highly electronegative atoms engaged in internal hydrogen bonding. In spite of the theoretical limitations, the present HF and MP2 minimum energy paths for protonated glycine have provided

important clues to the proton transfer mechanisms in amino acids and peptides.

ACKNOWLEDGMENT

We thank Dr. Alan D. Isaacson for many helpful discussions and Dr. S. Mark Cybulski for assistance with the IBM RS/6000 computer. Computations were supported by the Miami University Computing and Information Services, the Ohio Supercomputer Center, and the Ohio Board of Regents Separation Science Consortium. This work was supported by a grant from the National Institute of General Medical Sciences (R15-GM52670-01).

APPENDIX

Supplementary data to support several topics of discussion are provided sequentially from A1−A3 below. These data are drawn from published and unpublished work.

(A1) Formamide, H_2NCHO, is a model system for the peptide linkage. The smaller molecular size allows IRC calculations for proton transfer in a protonated formamide using a larger basis set at both the HF and MP2 levels. The IRCs optimized at the HF/6-31G*, HF/6-311+G**, MP2/6-31G*, and MP2/6-311+G** levels show PECs of similar shapes following a similar transfer path N···H−O (product) ↔ N···H···O (TS) ↔ N−H···O (reactant). This is an example where similar IRCs are produced regardless of basis size or correlation level. At the MP2/6-311+G** optimized level, the ΔE_0 (kcal/mol) for estimating proton transfer barriers are O-protonated product (planar with the O-H bond trans to the C−H bond) 0.0; TS 49.3; and N-protonated reactant 10.1. The ΔE_0 (kcal/mol) for estimating the GB of formamide are O-protonation (planar with the O−H bond cis to the C−H bond) 0.0; and N-protonation 13.8. The GB of N-protonation is estimated to be ca. 14 kcal/mol lower than that of O-protonation.

(A2) At the MP2/6-31G* optimized level the E_e (hartrees) for $GlyGlyH^+$ structure **5**−**8** of Figure 1 are −491.409910, −491.401217, −491.3840778, and −491.356499, respectively, which correspond to ΔE_e (kcal/mol) of 0.0, 5.5, 16.2, and 33.5. At the HF/6-31G* optimized level (ref 24) the respective E_e are −490.013141, −490.010444, −489.984294, and −489.970277, and the respective ΔE_e are 0.0, 1.7, 18.1, and 26.9. The E_e of GlyGly (structure **4** of ref 24) are −491.038983 and −489.645401 at the respective MP2/6-31G* and HF/6-31G* optimized levels.

(A3) Several $GlyH^+$ structures in ref 31 are of interest: the lowest-energy asymmetric and symmetric N-protonated species 1m and 1n, the O-protonated minima 4m, 5m, and 6m, and the O-protonated transition states 4t, 5t, 6t, 7t, and 8t. ΔE_e (kcal/mol) at the MP2/6-311+G** optimized level are 1m 0.00, 1n 0.13, 4m 28.44, 4t 28.88, 5m 29.05, 6m 30.39, 5t 30.42, 6t 30.73, 7t 32.87, and 8t 34.80. NCCO (°) are: 1m 11, 1n 0, 4m −175, 4t 131, 5m 180, 6m 95, 5t 109, 6t 69, 7t 163, and 8t 70. HNCC (°) are 1m 87, 1n 119, 4m 102, 4t 91, 5m −65, 6m −66, 5t −63, 6t −76, 7t 5, and 8t −1. Interconversions established from MP2/6-31G* IRC calculations include 1m ⇄ 1n, 4m ⇄ 4t, 4m ⇄ 7t ⇄ 5m, 5m ⇄ 5t ⇄ 6m, 6m ⇄ 6t, and 6m ⇄ 8t ⇄ 1m.

Supporting Information Available: Electronic energies for protonated glycine structures calculated at different levels in Table S1; selected geometrical parameters for the protonated glycine structures optimized at the HF and MP2 levels using the cc-pVDZ (A*), 6-31G* (A), 6-31G** (B), and 6-31+G** (C) basis sets in Table S2; selected physical properties for protonated glycine structures calculated at the HF and MP2 optimized levels using the 6-31G*, 6-31G**, and 6-31+G** basis sets in Table S3; optimized geometries for the critical points on the HF/6-31G* and MP/6-31G* IRCs expressed as Z-matrices in Tables S4 and S5; summaries of reaction path following for the MP2/6-31G* IRC in the forward and reverse directions in Tables S6 and S7; energies at selected optimized points on the MP2/6-31G* IRC calculated at different levels in Table S8; and enthalpies, entropies, Gibbs free energies, and natural logarithms of equilibrium constant and rate constant for the proton transfer reaction in the temperature range 100−2000 K calculated at the HF/6-31G* level in Figure S1. This material is available free of charge via the Internet at http://pubs.acs.org.

REFERENCES AND NOTES

(1) Fersht, A. *Enzyme Structure and Mechanism*; W. H. Freeman: New York, 1985.
(2) *Spectroscopy and Dynamics of Elementary Proton Transfer in Polyatomic Systems*; Barbara, P. F., Trommsdorff, H. P., Eds.; Special Issue, *Chem. Phys.* **1989**, *136*, 153−360.
(3) *Proton Transfer in Hydrogen Bonded System*; NATO ASI Series B291; Bountis, T., Ed.; Plenum: New York, 1992.
(4) *Tunneling in Chemical Reactions*; Benderskii, V. A., Goldanskii, V. I., Jortner, J., Eds.; Special Issue, *Chem. Phys.* **1993**, *170*, 265−460.
(5) Kearley, G. J.; Fillaux, F.; Baron, M.-H.; Bennington, S.; Tomkinson, J. A New Look at Proton Transfer Dynamics Along the Hydrogen Bonds in Amides and Peptides. *Science* **1994**, *264*, 1285−1289.
(6) Pardo, L.; Mazurek, A. P. Osman, R. Computational Models for Proton Transfer in Biological Systems. *Int. J. Quantum Chem.* **1990**, *37*, 701−711.
(7) Scheiner, S.; Wang, L. Hydrogen Bonding and Proton Transfers of the Amide Group. *J. Am. Chem. Soc.* **1993**, *115*, 1958−1963.
(8) Isaacson, A. D.; Wang, L.; Scheiner, S. Variational Transition State Theory Calculation of Proton Transfer Dynamics in $(H_3CH\cdots CH_3)^-$. *J. Phys. Chem.* **1993**, *97*, 1765−1769.
(9) Florián, J.; Hrouda, V.; Hobza, P. Proton Transfer in the Adenine-Thymine Base Pair. *J. Am. Chem. Soc.* **1994**, *116*, 1457−1460.
(10) Chipot, C.; Gorb, L. G.; Rivail, J.-L. Proton Transfer in the Mono- and the Dihydrated Complexes of HF and HCl: An MP2/6-31+G** Ab Initio Study in the Self-Consistent Reaction Field Model of Solvation. *J. Phys. Chem.* **1994**, *98*, 1601−1607.
(11) No, K. T.; Cho, K. H.; Kwon, O. Y.; Jhon, M. S.; Scheraga, H. A. Determination of Proton Transfer Energies and Lattice Energies of Several Amino Acid Zwitterions. *J. Phys. Chem.* **1994**, *98*, 10742−10749.
(12) Nguyen, M.-T.; Jamka, A. J.; Cazar, R. A.; Tao, F.-M. Structure and Stability of the Nitric Acid-Ammonia Complex in the Gas Phase and in Water. *J. Chem. Phys.* **1997**, *106*, 8710−8717.
(13) Bernasconi, C. F.; Wenzel, P. J.; Keeffe, J. R.; Gronert, S. Intrinsic Barriers and Transition State Structures in the Gas Phase Carbon-to-Carbon Identity Proton Transfers from Nitromethane to Nitromethide Anion and from Protonated Nitromethane to *aci*-Nitromethane. An Ab Initio Study. *J. Am. Chem. Soc.* **1997**, *119*, 4008−4020.
(14) Gorb, L.; Leszczynski, J. Intramolecular Proton Transfer in Mono- and Dihydrated Tautomers of Guanine: An ab Initio Post Hartree-Fock Study. *J. Am. Chem. Soc.* **1998**, *120*, 5024−5032.
(15) Chung, K.; Hedges, R. M.; Macfarlane, R. D. Theoretical Study of the Protonation of Glycine in Gas-Phase Ion-Molecule Reactions. *J. Am. Chem. Soc.* **1976**, *98*, 7523−7525.
(16) Wright, L. R.; Borkman, R. F.; Gabriel, A. M. Protonation of Glycine: An Ab Initio Self-Consistent Field Study. *J. Phys. Chem.* **1982**, *86*, 3951−3956.
(17) Jensen, J. H.; Gordon, M. S. The Conformational Potential Energy Surface of Glycine: A Theoretical Study. *J. Am. Chem. Soc.* **1991**, *113*, 7917−7924.
(18) Frey, R. F.; Coffin, J.; Newton, S. Q.; Ramek, M.; Chang, V. K. W.; Momany, F. A.; Schäfer, L. Importance of Correlation-Gradient Geometry Optimization for Molecular Conformational Analyses. *J. Am. Chem. Soc.* **1992**, *114*, 5369−5377.
(19) Jensen, F. Structure and Stability of Complexes of Glycine and Glycine Methyl Analogues with H^+, Li^+, and Na^+. *J. Am. Chem. Soc.* **1992**, *114*, 9533−9537.
(20) Császár, A. G. Conformers of Gaseous Glycine. *J. Am. Chem. Soc.* **1992**, *114*, 9568−9575.

(21) Bouchonnet, S.; Hoppilliard, Y. Proton and Sodium Ion Affinities of Glycine and Its Sodium Salt in the Gas Phase. Ab Initio Calculations. *Org. Mass Spectrom.* **1992**, *27*, 71−76.
(22) Hu, C.-H.; Shen, M.; Schaefer, H. F., III. Glycine Conformational Analysis. *J. Am. Chem. Soc.* **1993**, *115*, 2923−2929.
(23) Wu, Z.; Lebrilla, C. B. Gas-Phase Basicities and Sites of Protonation of Glycine Oligomers (GLY_n; n = 1−5). *J. Am. Chem. Soc.* **1993**, *115*, 3270−3275.
(24) Zhang, K.; Zimmerman, D. M.; Chung-Phillips, A.; Cassady, C. J. Experimental and Ab Initio Studies of the Gas-Phase Basicities of Polyglycines. *J. Am. Chem. Soc.* **1993**, *115*, 10812−10822.
(25) Baron, V.; Adamo, C.; Leij, F. Conformational Behavior of Gaseous Glycine by a Density Functional Approach. *J. Chem. Phys.* **1995**, *102*, 364−370.
(26) Tortonda, F. R.; Pascual-Ahuir, J. L.; Silla, E.; Tuñón, I. Why is Glycine a Zwitterion in Aqueous Solution? A Theoretical Study of Solvent Stabilizing Factors. *Chem. Phys. Lett.* **1996**, *260*, 21−26.
(27) Uggerud, E. The Unimolecular Chemistry of Protonated Glycine and the Proton Affinity of Glycine: A Computational Model. *Theor. Chem. Acc.* **1997**, *97*, 313−316.
(28) Okuyama-Yoshida, N.; Nagaoka M.; Yamabe, T. Potential Energy Function for Intramolecular Proton Transfer Reaction of Glycine in Aqueous Solution. *J. Phys. Chem.* **1998**, *102*, 285−292.
(29) Zhang, K.; Chung-Phillips, A. Gas-Phase Basicity of Glycine: A Comprehensive ab Initio Study. *J. Phys. Chem.* **1998**, *102*, 3625−3634.
(30) Tunón, I.; Silla, E.; Millot, C. Martins-Costa, M. T. C.; Ruiz-López, M. F. Intramolecular Proton Transfer of Glycine in Aqueous Solution Using Quantum Mechanics-Molecular Mechanics Simulations. *J. Phys. Chem. A* **1998**, *102*, 8673−8678.
(31) Zhang, K.; Chung-Phillips, A. Conformers of Gaseous Protonated Glycine. *J. Comput. Chem.* **1998**, *19*, 1862−1876.
(32) Zhang, K.; Cassady, C. J.; Chung-Phillips, A. Ab Initio Studies of Neutral and Protonated Triglycines: Comparison of Calculated and Experimental Gas-Phase Basicity. *J. Am. Chem. Soc.* **1994**, *116*, 11512−11521.
(33) Cassady, C. J.; Carr, S. R.; Zhang, K.; Chung-Phillips, A. Experimental and Ab Initio Studies on Protonations of Alanine and Small Peptides of Alanine and Glycine. *J. Org. Chem.* **1995**, *60*, 1704−1712.
(34) Halgren, T. S.; Lipscomb, W. N. The Synchronous-Transit Method for Determining Reaction Pathways and Locating Molecular Transition States. *Chem. Phys. Lett.* **1977**, *49*, 225−232.
(35) Gonzalez, C.; Schlegel, H. B. An Improved Algorithm for Reaction Path Following. *J. Chem. Phys.* **1989**, *90*, 2154−2161; Reaction Path Following in Mass-Weighted Internal Coordinates. *J. Phys. Chem.* **1990**, *94*, 5523−5527.
(36) Hehre, W. J.; Radom, L.; Schleyer, P. v. R.; Pople, J. A. *Ab Initio Molecular Orbital Theory*; John Wiley & Sons, New York, 1986.
(37) Frisch, M. J.; Trucks, G. W.; Schlegel, H. B.; Gill, P. M. W.; Johnson, B. G.; Robb, M. A.; Cheeseman, J. R.; Keith, T.; Petersson, G. A.; Montgomery. J. A.; Raghavachari, K.; Al-Laham, M. A.; Zakrzewski, V. G.; Ortiz, J. V.; Foresman, J. B.; Cioslowski, J.; Stefanov, B. B.; Nanayakkara, A.; Challacombe, M.; Peng, C. Y.; Ayala, P. Y.; Chen, W.; Wong, M. W.; Andres, J. L.; Replogle, E. S.; Gomperts, R.; Martin, R. L.; Fox, D. J.; Binkley, J. S.; Defrees, D. J.; Baker, J.; Stewart, J. J. P.; Head-Gordon, M.; Gonzalez, C.; Pople, J. A. *Gaussian 94*; Gaussian: Pittsburgh, 1994.
(38) See, e.g.: Purvis III, G. D.; Bartlett, R. J. A Full Coupled-Cluster Singles and Doubles Model: The Inclusion of Disconnected Triples. *J. Chem. Phys.* **1982**, *76*, 1910−1918.
(39) Lee, C.; Yang, W.; Parr, R. G. Development of the Colle-Salvetti Correlation Energy Formula into a Functional of the Electron Density. *Phys. Rev. B* **1988**, *37*, 785−789, and references cited therein.
(40) Wilson, A. K.; Dunning, T. H., Jr. Benchmark Calculations with Correlated Molecular Wave Functions. X. Comparison with "Exact" MP2 Calculations on Ne, HF, H_2O, and N_2. *J. Chem. Phys.* **1997**, *106*, 8718−8726, and references cited therein.
(41) Lee, T. J.; Taylor, P. R. A Diagnostic for Determining the Quality of Single-Reference Electron Correlation Methods. *Int. J. Quantum Chem.* **1989**, *S23*, 199−207.
(42) Steinfield, J. I.; Francisco J. S.; Hase, W. L. *Chemical Kinetic and Dynamics*; Prentice-Hall: Englewood Cliffs, NJ, 1989; Chapter 10, pp 308−339.
(43) Wigner, E. Overlapping of Potential Thresholds in Chemical Reactions. *Z. Phys. Chem.* **1932**, *B19*, 203−216.
(44) Mckee, M. L.; Page, M. Computing Reaction Pathways on Molecular Potential Energy Surfaces. Reviews in *Computational Chemistry*, Lipkowitz, K. B., Boyd, D. B., Eds.; VCH Publishers, Inc.: New York,1993; Vol. 4, pp 35−65.
(45) Hunter, E. P.; Lias S. G. Evaluated Gas-Phase Basicities and Proton Affinities of Molecules: An Update. *J. Phys. Chem. Ref. Data* (to be published). See, also: NIST Standard Reference Database Number 69; Mallard, W. G., Linstrom, P. J., Eds.; National Institute of Standards and Technology: Gaithersburg, MD, 1998.
(46) Hammond, G. S. A Correlation of Reaction Rates. *J. Am. Chem. Soc.* **1955**, *77*, 334−338.
(47) Del Bene, J. E.; Aue, D. H.; Shavitt, I. Stabilities of Hydrocarbons and Carbocations. 1. A Comparison of Augmented 6-31G, 6-311G, and Correlation Consistent Basis Sets. *J. Am. Chem. Soc.* **1992**, *114*, 1631−1640.
(48) Del Bene, J. E.; Person, W. B.; Szczepaniak, K. Properties of Hydrogen-Bonded Complexes Obtained from the B3LYP Functional with 6-31G(d,p) and 6-31+G(d,p) Basis Sets: Comparison with MP2/6-31+G(d,p) Results and Experimental Data. *J. Phys. Chem.* **1995**, *99*, 10705−18707.
(49) Curtiss, L. A.; Raghavachari, K.; Pople, J. A. *J. Chem. Phys.* **1993**, 1293−1298.
(50) Bolton, E. E.; Laidig, W. D.; Schleyer, P. v. R.; and Schaefer III, H. F. Singlet $C_2H_2Li_2$: Acetylenic and 1,2-Dilithioethene Isomers. A Remarkably Congested Potential Energy Hypersurface for a Simple Organometallic System. *J. Am. Chem. Soc.* **1994**, *116*, 9602−9612, and references cited.
(51) See, e.g.: Laidig, W. D.; Saxe, P.; Bartlett, R. J. The Description of N_2 and F_2 Potential Energy Surfaces Using Multireference Coupled Cluster Theory. *J. Chem. Phys.* **1986**, *86*, 887−907.
(52) Del Bene, J. E. Proton Affinities of NH_3, H_2O, and HF and Their Anions: A Quest for the Basis-Set Limit Using the Dunning Augmented Correlation-Consistent Basis Sets. *J. Phys. Chem.* **1993**, *97*, 107−110.
(53) Truong, T. N.; Duncan, W. A New Direct Ab Initio Dynamics Method for Calculating Thermal Rate Constants from Density Functional Theory. *J. Chem. Phys.* **1994**, *101*, 7408−7414.
(54) Pople, J. A.; Head-Gordon, M.; Raghavachari, K. Quadratic Configuration Interaction. A Geneneral Technique for Determining Electron Correlation Energies. *J. Chem. Phys.* **1987**, *87*, 5968−5975, and references cited.

CI9802225